

Multi-Task Learning for Routing Problem with Cross-Problem Zero-Shot Generalization

Fei Liu
fliu36-c@my.cityu.edu.hk
City University of Hong Kong
Hong Kong SAR

Xi Lin
xi.lin@my.cityu.edu.hk
City University of Hong Kong
Hong Kong SAR

Qingfu Zhang
qingfu.zhang@cityu.edu.hk
City University of Hong Kong
Hong Kong SAR

Xialiang Tong
tongxialiang@huawei.com
Huawei Noah's Ark Lab
Shenzhen, China

ABSTRACT

Vehicle routing problems (VRPs), which can be found in numerous real-world applications, have been an important research topic for several decades. Recently, the neural combinatorial optimization (NCO) approach that leverages a learning-based model to solve VRPs without manual algorithm design has gained substantial attention. However, current NCO methods typically require building one model for each routing problem, which significantly hinders their practical application for real-world industry problems with diverse attributes. In this work, we make the first attempt to tackle the crucial challenge of cross-problem generalization. In particular, we formulate VRPs as different combinations of a set of shared underlying attributes and solve them simultaneously via a single model through attribute composition. In this way, our proposed model can successfully solve VRPs with unseen attribute combinations in a zero-shot generalization manner. Extensive experiments are conducted on eleven VRP variants, benchmark datasets, and industry logistic scenarios. The results show that the unified model demonstrates superior performance in the eleven VRPs, reducing the average gap to around 5% from over 20% in the existing approach and achieving a significant performance boost on benchmark datasets as well as a real-world logistics application.

CCS CONCEPTS

- **Applied computing** → Transportation; Supply chain management; • **Computing methodologies** → Machine learning.

KEYWORDS

Vehicle routing, Cross-problem generalization, Attribute composition, Multi-task learning

1 INTRODUCTION

The vehicle routing problem (VRP) is a crucial topic in combinatorial optimization and operation research. It is widely studied in academia and has significant practical importance in real-world applications such as logistics, transportation, retail distribution, waste collection, and manufacturing [39]. The objective of the VRP is to optimally manage a fleet of vehicles, minimizing the total cost while satisfying the demands of customers. Real-world industry routing problems have diverse attributes (e.g., the capacities of vehicles, the time window constraints of requests), which result in numerous VRP variants [5, 43]. Developing a separate algorithm for each VRP

Mingxuan Yuan
yuan.mingxuan@huawei.com
Huawei Noah's Ark Lab
Hong Kong SAR

is very costly and impractical. Therefore, it is desirable to build a single unified solver for solving VRPs, which can significantly reduce the overall management cost and improve operational efficiency for companies. A few attempts have been made to develop a unified heuristics [12, 36, 42], but they demand much algorithm design effort with domain knowledge from experts.

Neural combinatorial optimization (NCO) learns a neural network based heuristic to solve combinatorial optimization problems. This approach has received growing research attention due to its potential ability to generate high-quality solutions without much human effort [3, 26, 44]. However, existing NCO methods work in a single-task manner [1, 28]. In other words, they need to train a neural network model for each optimization problem. When the problem changes, another model must be trained from scratch, which inevitably leads to high computational costs. Some attempts to overcome this shortcoming include transfer learning and multiobjective learning [13, 29, 31, 49]. However, the neural network models generated by these works can only be used to solve problems whose instances have been used for training. In other words, generalization across different problems has not been well addressed.

This paper proposes a multi-task learning approach for cross-problem generalization on vehicle routing problems to tackle the challenge. We develop a unified neural network model with attribute composition to handle multiple VRPs which can be efficiently trained by reinforcement learning (RL) without any labeled solution. We show that the unified model can be used to solve VRP variants in a zero-shot manner significantly outperforming the existing approach. Our contributions are summarized as follows:

- We propose a novel learning-based method to tackle cross-problem generalization in VRPs. It treats the VRP variants as different combinations of a set of shared underlying attributes, and solves various VRPs simultaneously in an end-to-end multi-task learning manner. To the best of our knowledge, this is the first work to investigate cross-problem neural solvers for VRPs.
- We develop a unified attention model with an attribute composition block. The proposed model has a promising zero-shot generalization ability to handle any combination of the basic attributes.
- We achieve state-of-the-art (SOTA) cross-problem generalization performance on eleven routing problems. This results in reducing the average gap to around 5% from over 20% in

the existing approach. Further validation of our zero-shot generalization approach on real-world benchmark datasets and an industry logistic application demonstrates a notable performance boost.

2 RELATED WORK

2.1 Neural Combinatorial Optimization (NCO)

NCO [3, 26, 44] intends to automatically learn a neural network-based heuristic to solve the combinatorial optimization problem. Compared to the other approaches (e.g., exact methods and heuristics), it requires very little domain-specific knowledge and usually generates high-quality solutions significantly fast. As a result, it has gained much attention in the past decade [3].

There are mainly two groups of works along this line: end-to-end methods [2, 9, 23, 27, 33, 35, 44] and improvement-based methods [6, 6, 20, 25]. The former aims to construct a solution without any assistance from non-learning methods, while the latter incorporates additional algorithms to improve performance. In this paper, we focus on the end-to-end approach.

2.2 NCO for Vehicle Routing Problem (VRP)

NCO has been successfully applied to many vehicle routing problems, including traveling salesman problem (TSP) [2], capacitated VRP (CVRP) [33], VRP with time windows (VRPTW) [50], open VRP (OVRP) [40], VRP with pickup and delivery [30], and heterogeneous VRP [29]. A recent survey of the works on learning-based methods for different vehicle routing problems can be found in Li et al. [28].

Despite extensive studies, the existing works have been conducted in a single-task manner, in which an individual neural model is trained for each problem. The time-consuming training process for every new problem hinders their practical application. It should be noted that various VRPs have common underlying attributes. Nevertheless, these similarities and correlations have not been adequately studied in the context of NCO. Recently, Bi et al. [4], Jiang et al. [22] and Geisler et al. [16] explored robust optimization over multiple distributions. Several works [8, 11, 14, 15, 32, 35] studied generalization to large-scale problems, and Zhou et al. [51] considered generalization in terms of both problem size and distribution. However, the cross-problem generalization has not been studied for routing problems.

2.3 Multi-Task Learning and Zero-Shot Learning

Multi-task learning (MTL) tackles multiple related learning tasks in a single learning process. It has been widely studied in various research fields, including computer vision [47], bioinformatics [17], and natural language processing [10]. However, MTL has received limited attention on combinatorial optimization problems. Reed et al. [37] and Ibarz et al. [21] proposed a general agent capable of solving diverse tasks, including several combinatorial optimization problems. Wang and Yu [45] presented a multi-task learning method for combinatorial optimization problems with separate encoders and decoders. Nevertheless, their approach falls short with respect

to handling complicated VRPs, and they require revision or fine-tuning to solve new problems that were not previously encountered during training.

Zero-shot learning (ZSL) allows the recognition of previously unseen objects based on their shared semantic properties or attributes [34, 38, 46]. Our idea of learning on multiple VRPs with several underlying attributes and generalizing to unseen VRPs is similar to compositional ZSL [38], which composes novel problems out of known subparts or attributes. In the context of routing problems, the attributes introduce additional constraints to the solution generation process, distinguishing them from the features or labels investigated in computer vision tasks [38].

3 PROBLEM STATEMENT AND MOTIVATION

In this section, we begin by introducing the basic CVRP formulation and then demonstrate that other VRP variants can be considered as extensions of the basic CVRP by incorporating additional attributes. We denote a CVRP on an undirected graph $G = (V, E)$. $V = \{v_0, \dots, v_n\}$, where v_0 is the depot and v_1, \dots, v_n are n customers. $V_c = \{v_1, \dots, v_n\}$ is the customer set. For the i -th customer, there is a demand d_i . $E = \{e_{ij}\}, i, j \in \{1, \dots, n\}$ are the edges between every two nodes. For each edge e_{ij} , there is an associated cost (distance) c_{ij} . A fleet of homogeneous vehicles with a capacity of C is sent out from the depot to visit the customers and return to the depot. Each customer must be visited once. The objective is to minimize the total travel distance of all used vehicles.

Figure 1 shows that various VRPs can be regarded as extensions of CVRP by considering one or more attributes. For example, VRPTW is extended from CVRP by adding time windows, and OVRPTW involves both time windows and open route attributes.

Except for the capacity constraints (C), we involve the following attributes in this paper:

- **Time Windows (TW):** we denote the time window for the i -th node as $[e_i, l_i], i \in \{0, \dots, n\}$, where e_i and l_i are the early and late time windows. In addition, each node has a service time s_i . We consider hard time windows, i.e., the vehicle must visit the node i in the time range from e_i to l_i . If the vehicle arrives at node i earlier than e_i , the vehicle has to wait until e_i .
- **Open Routes (O):** open routes mean that the vehicle does not need to return to the depot after it services all the customers on its route.
- **Backhauls (B):** the classic CVRP assumes that all vehicles load demands at the depot and unload at customers. We call these customers, who require deliveries $d_i > 0$, linehaul customers. Correspondingly, backhaul customers are those customers that need pickup $d_i < 0$. We consider the VRP with mixed linehaul and backhaul customers, i.e., the order of linehaul and backhaul customers can be mixed up in each route.
- **Duration limits (L):** duration limits refer to the situation in which the total length of the routes cannot exceed some pre-set thresholds. It is commonly used in real-world application scenarios to maintain a reasonable workload for different routes. In our setting, we use the same duration limit for all routes.

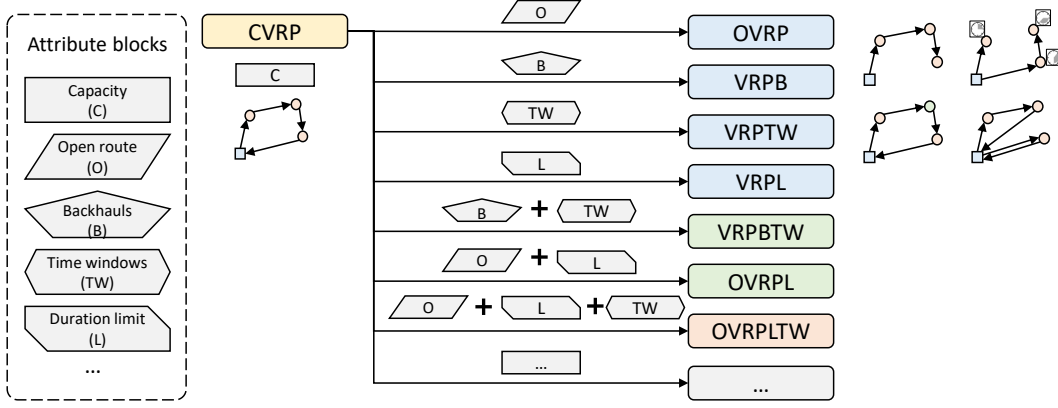


Figure 1: VRP variants as combinations of attribute blocks. The basic version is known as the Capacitated Vehicle Routing Problem (CVRP). VRP variants can be regarded as extensions of CVRP, encompassing additional attributes. For example, VRPTW extends CVRP by incorporating time windows, while OVRPLTW adds an open routes attribute alongside time windows.

Motivation In real-world industrial applications, there is a crucial demand to use a single model to solve various VRPs with different attributes. However, all current NCO methods need to build separate independent models to tackle these routing problems. Unlike previous approaches, this work treats the VRP variants as extensions of the basic CVRP with different combinations of the basic attributes (e.g., TW, O, B, and L). By leveraging the similarities and correlations among VRPs with shared underlying attributes, in this work, we propose to build the first cross-problem neural solver to solve various VRPs via a single model in a zero-shot generalization manner.

4 ATTRIBUTE-SHARING MODEL

We consider multiple VRPs as a set of related tasks and propose training a unified neural model through reinforcement learning to solve them simultaneously. Figure 2 illustrates the unified model used in this work. It consists of three parts: encoder, decoder, and attribute composition. We adopt the typical encoder-decoder framework of the Attention Model (AM) [26]. The encoder learns the node embeddings, and the decoder generates solutions sequentially. Different from the existing works [26, 27, 52], we enable its ability to handle various VRPs by adding an additional attribute composition block. The idea is that the diverse VRPs actually consist of several common underlying attributes. By learning from these attributes, we can solve an exponential number of new VRPs as any combination of them.

4.1 Model Structure

Encoder The encoder consists of N stacked multi-head attention (MHA) blocks [26]. The input of the encoder is the node features $f_i, i = 1, \dots, n$. In this paper, the input features for the i -th node are denoted as $f_i = \{x_i, d_i, e_i, l_i\}$, where x_i are the coordinates, d_i is the demand, and e_i and l_i are the early and late time windows, respectively. The input features are embedded through a linear projection to generate the initial feature embedding h_i . In each

MHA layer, skip connections [18] and instance normalization (IN) are used.

$$\begin{aligned} \hat{h}_i^{(l)} &= IN^l \left(h_i^{(l-1)} + MHA^{(l)} \left(h_1^{(l-1)}, \dots, h_n^{(l-1)} \right) \right), \\ h_i^{(l)} &= IN^l \left(\hat{h}_i + FF^l \left(\hat{h}_i \right) \right), \end{aligned} \quad (1)$$

where l and $l-1$ represent the current and last MHA layers, respectively. The FF contains a hidden sublayer with ReLU activations. The above encoding process generates the final node embeddings $h_i^{(N)}$. This encoding is performed only once, and the static node embeddings are reused for every decoding step.

Decoder The decoder constructs a solution sequentially. The input of the decoder includes three parts: the node embedding $h_1^{(N)}, \dots, h_n^{(N)}$, the embedding of currently visited node $h_t^{(N)}$, and the attribute embedding a_t . All the node embeddings are produced by the decoder. a_t is the embedding of the current state of attributes. We provide an attribute vector to include various attributes involved in multiple VRPs. At the t -th step, the attribute vector is $a_t = \{c_t, t_t, l_t, o_t\}$, where c_t is the remaining capacity of the current vehicle, t_t is the current time, l_t is the current duration of the route, and o_t indicates whether the route is open or not. Except for o_t , the others will be updated in each step. Backhauls are not embedded because they are implicitly considered in the node demands.

The decoder consists of one MHA layer and one single-head attention (SHA) layer with clipping. The MHA is slightly different from that used in the encoder. Skip connection, instance normalization, and FF sublayer are not used.

$$\begin{aligned} \hat{h}_c &= MHA_c \left(h_1^{(N)}, \dots, h_n^{(N)}, h_t^{(N)}, a_t \right), \\ u_1, \dots, u_n &= SHA_c \left(h_1^{(N)}, \dots, h_n^{(N)}, \hat{h}_c \right). \end{aligned} \quad (2)$$

The output embedding of MHA \hat{h}_c is used as the input of the SHA, and the SHA outputs the probabilities of choosing the next node using a softmax $p_i = \frac{e^{u_i}}{\sum_j e^{u_j}}$. We omit the step indicator t for

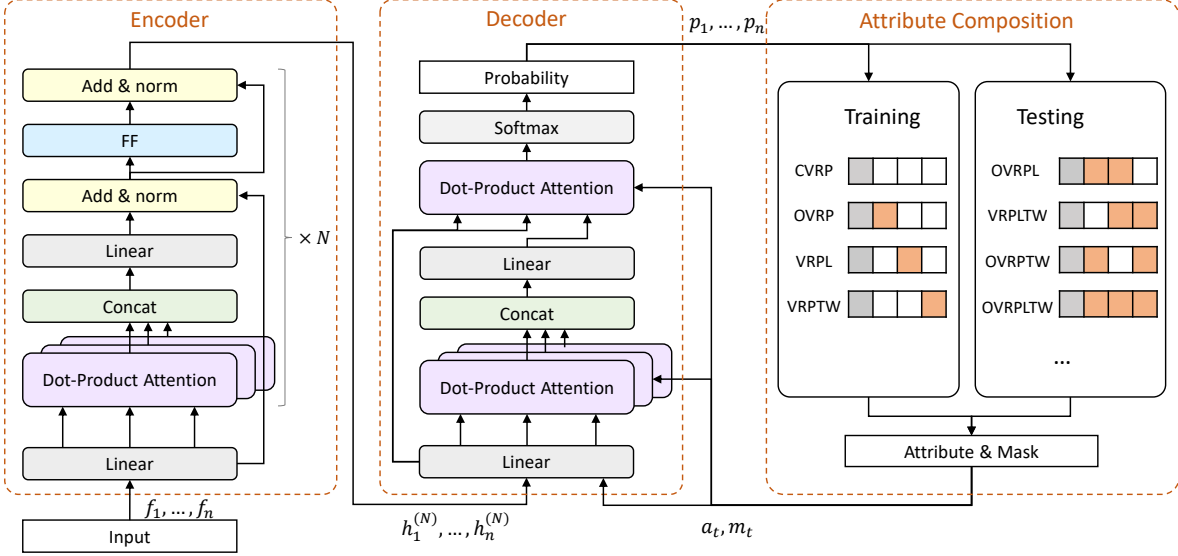


Figure 2: Unified model extended from attention model. The model is trained on multiple VRPs with diverse attributes. Then it can be used to solve numerous unseen VRPs as any combinations of the attributes involved in the training.

readability. The detailed structure of MHA and SHA can be found in Kool et al. [26].

In each step, we need to mask some nodes from being selected. We update a masking vector m_t . The associated positions of unwanted nodes in the vector will be set to -inf, which will be used in the attentions before softmax. Except for masking those nodes that have already been selected in the previous steps, the infeasibility caused by various attributes should also be considered. For example, these nodes that violate time window constraints should not be selected.

4.2 Attribute Composition

The input of the attribute composition is the input node features $f_i, i = 1, \dots, n$, the list of visited nodes V_t at the current step t , and the problem attributes A . The output is the attribute vector a_t and the mask vector m_t .

The problem attributes A are given explicitly with the input problem. A are used to activate the corresponding attribute updating procedure in the attribute composition block. In this paper, we have four procedures for the four attributes. Each procedure j updates the corresponding attribute in the attribute vector a_t^j and calculates an infeasible node list that must not be visited in the next step m_t^j . The output attribute vector will include all the updated activated attributes and pad the inactivated attributes to be a default value. The output mask vector m_t is the union of all activated attribute masks $m_t = V_t \cup \bigcup_{j \in A} m_t^j$. See Appendix A for the details of the attribute procedures.

For example, if only the capacity attribute is involved in the problem (i.e., CVRP), the indicator only activates the capacity updating procedure. In each step, the remaining capacity of the current vehicle is calculated. The attribute vector $a_t = \{c_t, t_t, l_t, o_t\}$ only updates c_t , and pads the rest attributes to zero. The infeasible nodes

that exceed vehicle capacity when added to the route are updated to update masking $m_t = V_t \cup m_t^c$.

Most of the investigated VRPs involve subsets of attributes in our unified model. We are learning the shared underlying attributes of diverse VRPs. In this way, we can train on a few VRPs and solve a much larger group of VRPs as arbitrary combinations of the underlying attributes. This characteristic enables the zero-shot generalization ability of our model.

4.3 Multi-Task Reinforcement Learning

We use the REINFORCE algorithm with a shared baseline following Kwon et al. [27]. We use greedy inference, i.e., a deterministic trajectory is constructed iteratively based on the policy. In each iteration, the next node is selected as the node with the maximum probability predicted by the decoder. n trajectories are constructed from n different starting points. Long-term rewards $R(\tau_1), \dots, R(\tau_n)$ (negative of the total distances) are calculated after the entire trajectories τ_1, \dots, τ_n are constructed. For the model with parameters θ , the following gradient ascent is used:

$$\nabla_{\theta} J(\theta) \approx \frac{1}{nB} \sum_{i=1}^B \sum_{j=1}^n \left(R(\tau_j^i | s_k^i) - b^i(s_k^i) \right) \nabla_{\theta} \log p_{\theta}(\tau_j^i | s_k^i), \quad (3)$$

where s_k represents the instances are generated from k -th task (VRP). $p_{\theta}(\tau_j^i)$ is the aggregation of the probability of selection in each step of the decoder. $b^i(s_k) = \frac{1}{n} \sum_{j=1}^n \left(R(\tau_j^i) \right)$ is the shared baseline. B is the batch size.

For multi-task learning, many optimizers have been designed to improve robustness and convergence. Instead of using sophisticated multi-task optimizers [7, 24, 48], we simply trained the multiple tasks with equal weight.

5 EXPERIMENTS

We conduct experiments on eleven vehicle routing problems, namely CVRP, VRPTW, OVRP, VRPB, VRPL, VRPBTW, VRPBL, OVRPL, OVRPLTW, OVRPBTW, and OVRPBLTW, along with benchmark datasets and our real-world logistic application cases. We train a unified model on the former five VRPs simultaneously and use the model to solve the rest problems in a zero-shot manner. Many of these routing problems are being addressed by the neural method for the first time. Note that one can easily extend the model to consider other attributes. We chose these attributes because they are among the most frequently used ones [5].

Instance Generation We use the same problem setup as that used in Kool et al. [26] to generate the basic CVRP. For VRPTW, we use the method introduced in Zhao et al. [50] to generate time windows and service times. For the rest problems, there is no existing work that solves exactly the same settings. We make the following settings: For VRPB, we first generate a CVRP and then randomly select 20% of customers as backhaul customers, whose demands are set to be the negative values of the original demands. For OVRP, we only need to set the open route indicator as active. For VRPL, the same maximum duration limit of 3 is used for each route.

Model Setting The number of MHA for the encoder is 6, and the number of heads is 8. The hidden layer size is 512, and the embedding size is 128.

Training In training, we randomly select one type of VRP in each batch and generate instances of the selected VRP. We use 10,000 training instances for each epoch with a batch size of 64, and the number of epochs for training is 10,000. Adam optimizer is used. The initial learning rate is 1e-4 with a weight decay of 1e-6. We implement the unified model using PyTorch, and the experiments are running on a single RTX 2080Ti GPU. Training on the vehicle routing problems of size 100 costs about ten days.

5.1 Results on Eleven VRPs

We initially provide an overall performance comparison on all eleven VRPs and then introduce detailed settings and results on both the training and unseen VRPs.

Figure 3 compares the performance in terms of the average gap (%) to the baseline solver hybrid genetic search (HGS) [42]. 5,000 instances of size 50 are used for each problem. The box plot on the left displays the overall performance, while the radar plot on the right illustrates the average gap on each VRP, with a smaller area indicating better results. The red one represents the results of our unified model trained through multi-task learning with attribute composition. The three compared models in different colors have the same encoder-decoder structure and training settings as our unified model. The difference is that they are trained on a single problem. ST_CVRP and ST_VRPTW were trained on CVRP and VRPTW, respectively, while ST_All was trained on OVRPBLTW with all attributes considered.

Our unified model significantly outperforms single-task learning models with an average gap of less than 4%. It demonstrates strong generalization capabilities across different VRPs. In comparison, single-task learning models only perform well on the training problem. For example, according to the results depicted in the radar plot, ST_All achieves promising performance on the problem it

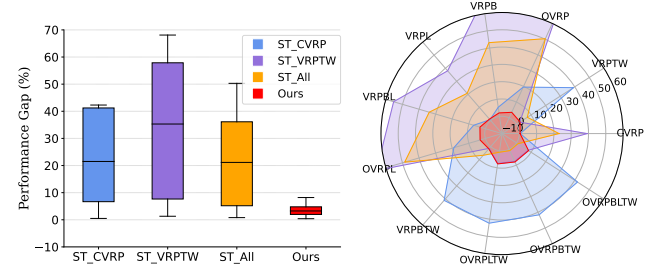


Figure 3: A comparison of gaps on eleven VRPs (Left: box plot, Right: radar plot). ST represents the unified model trained with single-task learning on CVRP, ST_all represents the unified model with single-task learning on OVRPBLTW, and MT represents our approach, i.e., the unified model with multi-task learning on five VRPs. ST_FT and MT_FT are the fine-tuning models.

was trained on (OVRPBLTW), as well as on two VRP variants with similar attributes (OVRPBTW and OVRPLTW), even slightly surpassing our unified model. However, its performance deteriorates significantly on the remaining VRPs. It suggests that training with all attributes fails to generalize effectively to other variants with only a subset of attributes.

5.1.1 Attribute Correlation. We conduct a comparison of the distributions of different routing problems on a two-dimensional reduction space to visualize and analyze the attribute correlation. We first extract the sample features from the decoder hidden layer of our unified model. Each sample feature is the decoder hidden layer embedding of one inference step. For each VRP, we collect 1,000 feature samples. All the feature samples from different VRPs are transformed into one two-dimensional reduction space using t-distributed Stochastic Neighbor Embedding (t-SNE).

Figure 4 shows a comparison of the distributions of five VRPs on the reduction space. There is a clear distinct distribution of VRPTW compared with others as the time window attribute poses a strong constraint over the route. In addition to VRPTW, OVRP also shows a different pattern than others because it does not force routes back to the depot presenting less constraint. In contrast, CVRP and VRPL follow a very close distribution and overlap with each other in most areas. This can be attributed to the fact that our route length limit is set to 3, which is easily satisfied in our settings.

We employ the Hausdorff distance to quantify the similarity between two VRPs in the reduced space. Figure 5 illustrates the Hausdorff distances of CVRP and OVRPBLTW (All) to other VRPs. The distances observed in the reduced space are consistent with the zero-shot generalization performance depicted in the radar plot in Figure 3, with further details provided in Appendix B. For instance, the model trained on CVRP exhibits a substantial distance from VRPs with time window constraints, correlating with its subpar performance on these problems. Furthermore, the optimal gap on VRPL coincides with the minimal distance between CVRP and VRPL.

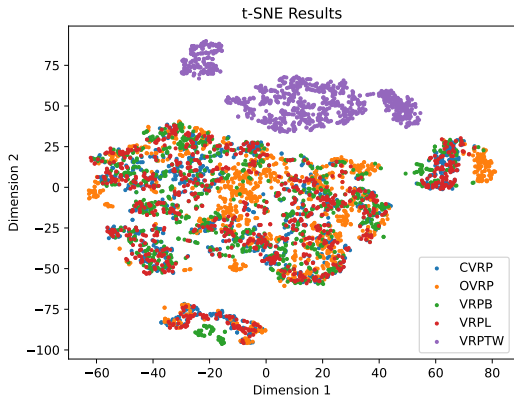


Figure 4: A comparison of distributions of different VRPs on two-dimensional reduction space of the decoder hidden layer.

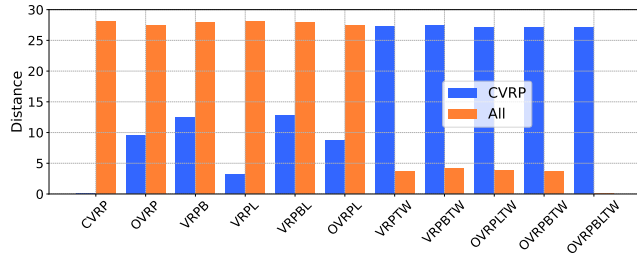


Figure 5: Hausdorff distance in reduction space comparing CVRP and OVRPBLTW (All) with other problems

Table 1: Training costs between POMO with single-task learning and our model with multi-task learning on five VRPs

	#Models	#Total Para.	#Total Epochs	Time Cost (day)
POMO	5	6.56M	50,000	49
Ours	1	1.35M	10,000	10.5

5.1.2 Training VRPs. Table 2 lists the experimental results on the five VRPs used in the training. For CVRP, we compare our results with the original version of AM [26] and SOTA extensions, namely, POMO [27], and GCAM [52]. For VRPTW, a deep reinforcement learning method (DRL) [50] and POMO are compared. The results of LHK3 [19] and Gurobi are used as the baseline for CVRP and VRPTW, respectively. For the rest three problems, there are no existing end-to-end NCO methods for comparison. We implement POMO on these problems and use the state-of-the-art hybrid genetic search (HGS) [42] solver as the baseline.

Table 2: Experimental results on five training VRPs. (The compared neural solvers require training one model for each VRP)

Problem	Method	N=50			N=100			
		Dis.	Gap	Time	Dis.	Gap	Time	
CVRP	HGS	10.38	-	7h	15.54	-	14h	
	LHK3	10.38	0.00%	7h	15.61	0.46%	14h	
	AM (Samp1280)	10.59	2.02%	7m	16.16	4.00%	30m	
	GCAM (Samp1280)	10.64	2.50%	-	16.29	4.83%	-	
	POMO	10.53	1.41%	3s	15.87	2.13%	10s	
	POMO (Aug8)	10.44	0.58%	15s	15.75	1.36%	1.1m	
	SGBS	10.39	0.12%	2.0m	15.63	0.62%	11.8m	
	Ours	10.56	1.73%	3s	15.90	2.29%	11s	
	Ours (Aug8)	10.47	0.85%	20s	15.80	1.71%	1.2m	
	Ours+SGBS	10.40	0.18%	2.3m	15.66	0.81%	12.6m	
VRPTW	HGS	16.30	-	7h	26.14	-	14h	
	LHK3	16.52	1.36%	7h	26.60	1.76%	14h	
	DRL (BS10)	17.90	9.82%	1m	29.50	12.85%	2m	
	DRL (BS10) +LNS	16.94	3.93%	11m	27.44	4.97%	65m	
	POMO	16.78	2.97%	3s	27.13	3.77%	11s	
	POMO (Aug8)	16.66	2.22%	19s	26.91	2.93%	1.2m	
	SGBS	16.55	1.52%	2.9m	26.55	1.58%	15.1m	
	Ours	16.96	4.06%	3s	27.46	5.05%	11s	
	Ours (Aug8)	16.80	3.09%	20s	27.13	3.81%	1.2m	
	Ours+SGBS	16.58	1.71%	3.2m	26.63	1.89%	17.9m	
OVRP	HGS	6.49	-	7h	9.71	-	14h	
	LHK3	6.52	0.46%	7h	9.75	0.41%	14h	
	POMO	6.73	3.67%	3s	10.18	4.91%	10s	
	POMO (Aug8)	6.63	2.14%	16s	10.07	3.76%	1.1m	
	SGBS	6.56	1.12%	2.1m	9.89	1.92%	12.1m	
	Ours	6.81	4.90%	3s	10.34	6.56%	11s	
	Ours (Aug8)	6.71	3.40%	20s	10.14	4.48%	1.2m	
	Ours+SGBS	6.59	1.58%	2.5m	9.94	2.38%	13.4m	
	VRPB	HGS	7.69	-	7h	11.13	-	14h
	LHK3	7.70	0.18%	7h	11.29	1.40%	14h	
VRPB	POMO	7.92	3.06%	3s	11.57	3.88%	10s	
	POMO (Aug8)	7.84	2.05%	15s	11.43	2.68%	1.1m	
	SGBS	7.78	1.22%	1.9m	11.31	1.59%	11m	
	Ours	8.17	6.36%	3s	11.72	5.23%	11s	
	Ours (Aug8)	7.87	2.40%	20s	11.53	3.58%	1.2m	
	Ours+SGBS	7.78	1.25%	2.1m	11.36	2.06%	11.7m	
	VRPL	HGS	10.37	-	7h	15.54	-	14h
	LHK3	10.37	0.03%	7h	15.61	0.43%	14h	
	POMO	10.55	1.78%	3s	15.84	1.96%	10s	
	POMO (Aug8)	10.46	0.91%	16s	15.72	1.14%	1.1m	
VRPL	SGBS	10.40	0.30%	2.3m	15.64	0.66%	13.1m	
	Ours	10.56	1.88%	3s	15.96	2.72%	11s	
	Ours (Aug8)	10.47	0.98%	20s	15.80	1.66%	1.2m	
	Ours+SGBS	10.40	0.33%	2.6m	15.67	0.83%	14.3m	
	Average	POMO	10.50	2.58%	3s	16.12	3.33%	10s
	POMO (Aug8)	10.41	1.58%	16s	15.97	2.37%	1.1m	
	SGBS	10.34	0.86%	2.24m	15.81	1.28%	12.6m	
	Ours	10.61	3.78%	3s	16.27	4.37%	11s	
	Ours (Aug8)	10.46	2.14%	20s	15.81	3.05%	1.2m	
	Ours+SGBS	10.35	1.01%	2.5m	15.85	1.59%	14.0m	

We extended the original POMO on these problems and trained these models independently on each problem with single-task learning. We keep the settings of the original paper [27]. For other compared single-task learning models, we select the best results from the corresponding papers. If additional inference techniques are

Table 3: Zero-shot generalization performance on five new VRPs.

VRP	Method	n50		n100		VRP	Method	n50		n100	
		Dis.	Gap	Dis.	Gap			Dis.	Gap	Dis.	Gap
VRPBL	HGS	7.70	-	11.15	-	OVRPLTW	HGS	10.69	-	17.35	-
	NI	11.69	51.86%	17.38	55.92%		NI	15.74	47.20%	26.16	50.78%
	FI	11.61	50.81%	16.37	46.88%		FI	15.22	42.41%	25.81	48.79%
	POMO_CVRP	8.21	6.61%	12.41	11.37%		POMO_CVRP	15.23	42.46%	26.75	54.18%
	POMO_VRPTW	13.43	74.45%	17.86	60.27%		POMO_VRPTW	11.51	7.70%	19.41	11.88%
	Ours	7.97	3.48%	11.65	4.50%		Ours	11.50	7.59%	19.34	11.50%
OVRPL	HGS	6.49	-	9.71	-	OVRPBTW	HGS	10.67	-	17.31	-
	NI	13.85	113.55%	13.61	40.17%		NI	15.76	47.77%	26.24	51.60%
	FI	14.34	121.11%	13.46	38.62%		FI	15.22	42.69%	25.79	48.99%
	POMO_CVRP	7.75	19.47%	11.78	21.35%		POMO_CVRP	15.25	42.98%	26.78	54.69%
	POMO_VRPTW	10.80	66.54%	18.62	91.78%		POMO_VRPTW	11.52	7.94%	19.48	12.51%
	Ours	6.69	3.10%	10.15	4.57%		Ours	11.49	7.72%	19.32	11.61%
VRPBTW	HGS	16.43	-	26.31	-	Average	HGS	10.39	-	16.36	-
	NI	18.92	15.15%	36.84	40.05%		NI	15.19	46.16%	24.05	46.95%
	FI	18.33	11.56%	36.59	39.10%		FI	14.95	43.78%	23.60	44.25%
	POMO_CVRP	22.98	39.85%	38.99	48.20%		POMO_CVRP	13.88	33.56%	23.34	42.64%
	POMO_VRPTW	16.63	1.22%	27.18	3.33%		POMO_VRPTW	12.78	22.93%	20.51	25.34%
	Ours	16.70	1.66%	27.11	3.05%		Ours	10.87	4.59%	17.51	7.03%

used, such as beam search (BS) and sampling (Samp), their size is indicated in the parentheses following the method. We adopt additional data augmentation (Aug) following POMO [27]. In addition, the advanced inference strategy simulation guided beam search (SGBS) has been investigated and integrated into our framework for better zero-shot generation performance.

Table 1 presents the required number of models and the total parameter sizes for single-task learning and our multi-task learning for five tasks. The required number of models (and the total parameters) could be much higher for single-task learning if we train a different model for each possible attribute combination, which is not affordable for real-world applications.

For each problem, the evaluations are conducted on 5,000 instances. We compare the performance with respect to three criteria: the average distance (Dis.), the gap of the average distance to the baseline results, and the total running time on 5,000 instances. In general, our unified model is competitive with the existing single-task NCO methods. On CVRP and VRPTW, the results are better than the various existing end-to-end methods except for POMO. The gap between our model and the optimal baselines is less than 5% across all five VRPs tested, and our running time is significantly less than the baseline methods. The average gap of our unified model on the five training VRPs can be further reduced to around 1% when integrating with SGBS, with an acceptable increase in inference time. Despite slightly inferior results compared to POMO and SGBS, we note that the latter requires training individual neural networks for each problem and does not generalize well on unseen problems.

5.1.3 Unseen VRPs. We use our unified model to solve unseen VRPs in a zero-shot manner. The experiments are carried out on five VRPs (i.e., VRPBTW, VRPBL, OVRPL, OVRPLTW, and OVRPBTW).

We compare the results of our unified model with single-task models, two commonly used constructive heuristics, and the SOTA heuristic HGS. The constructive heuristics are the nearest insertion method and farthest insertion method. We extended the source code of HGS so that it can solve these routing problems [42]. The two single-task models are POMO trained on CVRP and VRPTW, respectively. We added the masking procedure used in our unified model to POMO so that they are applicable to different VRPs. Our unified model and the two single-task models are used in a zero-shot way without any fine-tuning on the new VRPs.

Table 3 shows the zero-shot performance. The results are evaluated on 5,000 instances for each problem. Our unified model outperforms other methods including two heuristic methods except for HGS, which is specifically developed for VRPs. The two single-task models are inferior to our multi-task unified model. The deficiency of single-task models is more obvious in problems with very different attributes. For example, the model only trained on CVRP performs worse on these problems involving time windows attributes, while the model trained on VRPTW has poor performance on VRPBL. The average gap of our model over these five unseen VRPs is 4.6% and 7% on VRPs of sizes 50 and 100, respectively.

5.2 Benchmark Datasets

We apply our model on the well-known CVRPLib benchmark datasets to demonstrate the out-of-distribution performance. Most of them are derived from real-world instances and have diverse distributions and sizes. Specifically, we select six test suites with diverse attributes from CVRPLIB¹. There are a total of 181 instances whose problem size ranges from 30 to 1,000. We normalize the coordinates of customers so that they are within the unit range of [0, 1]. We also normalize the demands with respect to the vehicle capacity.

¹<http://vrp.atd-lab.inf.puc-rio.br/>

Table 4: Results on CVRPLib datasets with diverse distributions and sizes.

Benchmark	Size	BKS	POMO		Ours	
			Dis.	Gap	Dis.	Gap
Set A	31-79	1041.9	1104.8	6.0%	1066.8	2.4%
Set B	30-77	963.7	1065.7	10.6%	992.2	2.9%
Set F	44-134	707.7	770.6	8.9%	760.6	7.5%
Set M	100-199	1083.6	1145.2	5.7%	1141.9	5.4%
Set P	15-100	587.4	660.4	12.4%	627.1	6.8%
	100-300	33868.5	36299.07	7.2%	35954.7	6.2%
Set X	300-500	63774.8	71524.15	12.2%	68841.6	7.9%
	500-700	88561.4	107927.9	21.9%	98843.8	11.6%
	700-1000	113619.5	149858.6	31.9%	129270.9	13.8%

To evaluate the performance, we compare our unified model with POMO, which is trained on CVRP. Both models are trained on instances of size 100. We use the best-known solutions (BKS) provided by CVRPLIB as the baseline. The criteria for comparison include the average distance over all test suite instances and the average gap to BKS.

Table 4 lists the information of six test suites as well as the experimental results. The results demonstrate that, although our model is not specifically trained for CVRP, it outperforms POMO on all test suites. Overall, the average gap between our unified model and the BKS is less than 10%, which is about half of POMO.

We divide the 100 instances in X into four groups based on their problem size. The results of our model and POMO on each group are summarized in Table 4. Our findings indicate that both models perform similarly well on small-scale instances, but as the scale of the problem increases, the performance of POMO deteriorates. In fact, in the largest group, the average gap of POMO is over 30%. Conversely, our model is more robust across problem sizes, with its gap increasing only from 6.2% to 13.8%.

5.3 Industry Logistic Application

Finally, we validate the unified model on a real-world industry logistic application with three different cases. The test sets are derived from our historical cross-city transportation logistic data spanning 30 days. Three types of cases are examined. The first case involves the typical CVRP, where only the vehicle capacity constraint is taken into account. Three datasets containing instances of different vehicle capacities: large(L), middle(M), and small(S) were collected. These datasets consisted of a total of 64 instances, with customer numbers varying from 50 to 100 and demands ranging from 25 to the maximum vehicle capacity. In the second case OVRP, drivers are not required to return vehicles to the depot, resulting in an open route scenario. In the final case VRPL, the duration limit indicated by the route length is imposed on the drivers. In the last VRPL case, only one dataset is collected with the largest vehicle capacity, as duration limit constraints are typically not impactful on vehicles with small capacity. Table 5 lists the statistics of the industry logistic datasets.

We compared our unified model to models trained using single-task learning in a zero-shot manner, without any fine-tuning or adaptation. The three models under comparison were trained on

Table 5: Real-world logistic application instance statistics

Case	Size	Capacity	Open	Limit
			X	X
CVRP	SetA	50-100	L	X
	SetB	50-100	M	X
	SetC	50-100	S	X
OVRP	SetA	50-100	L	✓
	SetB	50-100	M	✓
	SetC	50-100	S	✓
VRPL	50-100	L	X	✓

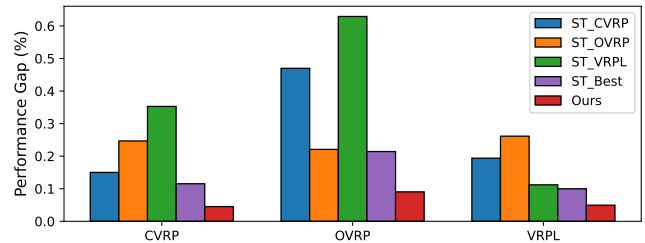


Figure 6: Results on real-world logistic application. CVRP, OVRP, and VRPL represent the three investigated application cases. ST_CVRP, ST_OVRP, and ST_VRPL represent the model trained on CVRP, OVRP, and VRPL, respectively. ST_Best denotes the average gaps of the best result among the three single-task learning models for each instance.

CVRP, OVRP, and VRPL datasets, respectively. Figure 6 depicts the average gaps to the baseline HGS in these three cases. For CVRP and OVRP, the results are averaged across all three sets. ST_Best denotes the average gaps of the best result among the three single-task learning models for each instance. Our unified model outperformed the best results of the compared models, achieving gaps of less than 5% on CVRP and VRPL, and 10% on OVRP.

6 CONCLUSION

This work has proposed a novel learning-based approach to solve various vehicle routing problems (VRPs) with different attributes by a single unified model. In our proposed framework, different VRPs are treated as different combinations of several shared basic attributes (e.g., time windows, open routes, backhauls, and duration limits). In this way, by leveraging the similarities and relations among different VRPs with shared underlying attributes, we can build a single unified model to tackle numerous VRPs in an end-to-end manner. To the best of our knowledge, this work is the first attempt to develop a cross-problem neural VRP solver, which is desirable for many real-world industrial applications. Experimental results demonstrate that our proposed model exhibits promising zero-shot generalization performance on unseen VRPs with new combinations of the basic attributes. Remarkably, without any fine-tuning, our model can outperform single-task models substantially, reducing the average performance gap from over 20% to approximately 5% across eleven VRPs, and achieving significant performance boost on benchmark datasets as well as a real-world logistics application.

REFERENCES

[1] Ruibin Bai, Xian Chen, Zhi-Long Chen, Tianxiang Cui, Shuhui Gong, Wentao He, Xiaoping Jiang, Huan Jin, Jiahuan Jin, Graham Kendall, et al. 2023. Analytics and machine learning in vehicle routing research. *International Journal of Production Research* 61, 1 (2023), 4–30.

[2] Irwan Bello, Hieu Pham, Quoc V Le, Mohammad Norouzi, and Samy Bengio. 2016. Neural combinatorial optimization with reinforcement learning. *arXiv preprint arXiv:1611.09940* (2016).

[3] Yoshua Bengio, Andrea Lodi, and Antoine Prouvost. 2021. Machine learning for combinatorial optimization: a methodological tour d’horizon. *European Journal of Operational Research* 290, 2 (2021), 405–421.

[4] Jieyi Bi, Yining Ma, Jiahai Wang, Zhiguang Cao, Jinbiao Chen, Yuan Sun, and Yeow Meng Chee. 2022. Learning Generalizable Models for Vehicle Routing Problems via Knowledge Distillation. *arXiv preprint arXiv:2210.07686* (2022).

[5] Kris Braeckers, Katrien Ramaekers, and Inneke Van Nieuwenhuysse. 2016. The vehicle routing problem: State of the art classification and review. *Computers & industrial engineering* 99 (2016), 300–313.

[6] Xinyun Chen and Yuandong Tian. 2019. Learning to perform local rewriting for combinatorial optimization. *Advances in Neural Information Processing Systems* 32 (2019).

[7] Zhao Chen, Vijay Badrinarayanan, Chen-Yu Lee, and Andrew Rabinovich. 2018. Gradnorm: Gradient normalization for adaptive loss balancing in deep multitask networks. In *International conference on machine learning*. PMLR, 794–803.

[8] Hanni Cheng, Haosi Zheng, Ya Cong, Weihao Jiang, and Shiliang Pu. 2023. Select and Optimize: Learning to solve large-scale TSP instances. In *Proceedings of The 26th International Conference on Artificial Intelligence and Statistics (Proceedings of Machine Learning Research, Vol. 206)*, Francisco Ruiz, Jennifer Dy, and Jan-Willem van de Meent (Eds.). PMLR, 1219–1231.

[9] Jinho Choo, Yeong-Dae Kwon, Jihoon Kim, Jeongwoo Jae, André Hottung, Kevin Tierney, and Youngjune Gwon. 2022. Simulation-guided beam search for neural combinatorial optimization. *Advances in Neural Information Processing Systems* 35 (2022), 8760–8772.

[10] Roman Collobert and Jason Weston. 2008. A unified architecture for natural language processing: Deep neural networks with multitask learning. In *Proceedings of the 25th international conference on Machine learning*, 160–167.

[11] Darko Drakulic, Sofia Michel, Florian Mai, Arnaud Sors, and Jean-Marc Andreoli. 2023. BQ-NCO: Bisimulation Quotienting for Generalizable Neural Combinatorial Optimization. *arXiv preprint arXiv:2301.03313* (2023).

[12] Najib Errami, Eduardo Queiroga, Ruslan Sadykov, and Eduardo Uchoa. 2023. VRPSolverEasy: a Python library for the exact solution of a rich vehicle routing problem. (2023).

[13] Liang Feng, Yuxiao Huang, Ivor W Tsang, Abhishek Gupta, Ke Tang, Kay Chen Tan, and Yew-Soo Ong. 2020. Towards faster vehicle routing by transferring knowledge from customer representation. *IEEE Transactions on Intelligent Transportation Systems* 23, 2 (2020), 952–965.

[14] Zhang-Hua Fu, Kai-Bin Qiu, and Hongyuan Zha. 2021. Generalize a small pre-trained model to arbitrarily large tsp instances. In *Proceedings of the AAAI Conference on Artificial Intelligence*, Vol. 35. 7474–7482.

[15] Chengrui Gao, Haopu Shang, Ke Xue, Dong Li, and Chao Qian. 2023. Towards Generalizable Neural Solvers for Vehicle Routing Problems via Ensemble with Transferrable Local Policy. *arXiv:2308.14104* [cs.LG]

[16] Simon Geisler, Johanna Sommer, Jan Schuchardt, Aleksandar Bojchevski, and Stephan Günnemann. 2022. Generalization of Neural Combinatorial Solvers Through the Lens of Adversarial Robustness. *arXiv:2110.10942* [cs.LG]

[17] Dan He, David Kuhn, and Laxmi Parida. 2016. Novel applications of multitask learning and multiple output regression to multiple genetic trait prediction. *Bioinformatics* 32, 12 (2016), i37–i43.

[18] Kaiming He, Xiangyu Zhang, Shaoqing Ren, and Jian Sun. 2016. Deep residual learning for image recognition. In *Proceedings of the IEEE conference on computer vision and pattern recognition*, 770–778.

[19] Keld Helsgaun. 2017. An extension of the Lin-Kernighan-Helsgaun TSP solver for constrained traveling salesman and vehicle routing problems. *Roskilde: Roskilde University* 12 (2017).

[20] André Hottung and Kevin Tierney. 2019. Neural large neighborhood search for the capacitated vehicle routing problem. *arXiv preprint arXiv:1911.09539* (2019).

[21] Borja Ibarz, Vitaly Kurin, George Papamakarios, Kyriacos Nikiforou, Mehdi Bennani, Róbert Csordás, Andrew Joseph Dudzik, Matko Bošnjak, Alex Vitvitsky, Yulia Rubanova, et al. 2022. A generalist neural algorithmic learner. In *Learning on Graphs Conference*. PMLR, 2–1.

[22] Yuan Jiang, Yaoxin Wu, Zhiguang Cao, and Jie Zhang. 2022. Learning to solve routing problems via distributionally robust optimization. In *Proceedings of the AAAI Conference on Artificial Intelligence*, Vol. 36. 9786–9794.

[23] Chaitanya K Joshi, Quentin Cappart, Louis-Martin Rousseau, and Thomas Laurent. 2022. Learning the travelling salesperson problem requires rethinking generalization. *Constraints* 27, 1-2 (2022), 70–98.

[24] Alex Kendall, Yarin Gal, and Roberto Cipolla. 2018. Multi-task learning using uncertainty to weigh losses for scene geometry and semantics. In *Proceedings of the IEEE conference on computer vision and pattern recognition*. 7482–7491.

[25] Wouter Kool, Herke van Hoof, Joaquin Gromicho, and Max Welling. 2022. Deep policy dynamic programming for vehicle routing problems. In *Integration of Constraint Programming, Artificial Intelligence, and Operations Research: 19th International Conference, CPAIOR 2022, Los Angeles, CA, USA, June 20–23, 2022, Proceedings*. Springer, 190–213.

[26] Wouter Kool, Herke Van Hoof, and Max Welling. 2018. Attention, learn to solve routing problems! *arXiv preprint arXiv:1803.08475* (2018).

[27] Yeong-Dae Kwon, Jinho Choo, Byoungjin Kim, Iljoo Yoon, Youngjune Gwon, and Seungjai Min. 2020. Pomo: Policy optimization with multiple optima for reinforcement learning. *Advances in Neural Information Processing Systems* 33 (2020), 21188–21198.

[28] Bingjie Li, Guohua Wu, Yongming He, Mingfeng Fan, and Witold Pedrycz. 2022. An overview and experimental study of learning-based optimization algorithms for the vehicle routing problem. *IEEE/CAA Journal of Automatica Sinica* 9, 7 (2022), 1115–1138.

[29] Jingwen Li, Yining Ma, Ruize Gao, Zhiguang Cao, Andrew Lim, Wen Song, and Jie Zhang. 2021. Deep reinforcement learning for solving the heterogeneous capacitated vehicle routing problem. *IEEE Transactions on Cybernetics* 52, 12 (2021), 13572–13585.

[30] Jingwen Li, Liang Xin, Zhiguang Cao, Andrew Lim, Wen Song, and Jie Zhang. 2021. Heterogeneous attentions for solving pickup and delivery problem via deep reinforcement learning. *IEEE Transactions on Intelligent Transportation Systems* 23, 3 (2021), 2306–2315.

[31] Xi Lin, Zhiyuan Yang, and Qingfu Zhang. 2022. Pareto Set Learning for Neural Multi-Objective Combinatorial Optimization. In *International Conference on Learning Representations*.

[32] Sahil Manchanda, Sofia Michel, Darko Drakulic, and Jean-Marc Andreoli. 2023. On the Generalization of Neural Combinatorial Optimization Heuristics. In *Machine Learning and Knowledge Discovery in Databases: European Conference, ECML PKDD 2022, Grenoble, France, September 19–23, 2022, Proceedings, Part V*. Springer, 426–442.

[33] Mohammadreza Nazari, Afshin Oroojlooy, Lawrence Snyder, and Martin Takáć. 2018. Reinforcement learning for solving the vehicle routing problem. *Advances in neural information processing systems* 31 (2018).

[34] Junhyuk Oh, Satinder Singh, Honglak Lee, and Pushmeet Kohli. 2017. Zero-shot task generalization with multi-task deep reinforcement learning. In *International Conference on Machine Learning*. PMLR, 2661–2670.

[35] Xuanhao Pan, Yan Jin, Yuandong Ding, Mingxiao Feng, Li Zhao, Lei Song, and Jiang Bian. 2023. H-TSP: Hierarchically Solving the Large-Scale Traveling Salesman Problem. In *AAAI 2023*.

[36] Bochra Rabbouch, Fouad Saâdaoui, and Rafaa Mraibi. 2021. Efficient implementation of the genetic algorithm to solve rich vehicle routing problems. *Operational Research* 21 (2021), 1763–1791.

[37] Scott Reed, Konrad Zolna, Emilio Parisotto, Sergio Gomez Colmenarejo, Alexander Novikov, Gabriel Barth-Maron, Mai Gimenez, Yury Sulsky, Jackie Kay, Jost Tobias Springenberg, et al. 2022. A generalist agent. *arXiv preprint arXiv:2205.06175* (2022).

[38] Frank Ruis, Gertjan Burghouts, and Doina Bucur. 2021. Independent prototype propagation for zero-shot compositionality. *Advances in Neural Information Processing Systems* 34 (2021), 10641–10653.

[39] Paolo Toth and Daniela Vigo. 2014. *Vehicle routing: problems, methods, and applications*. SIAM.

[40] Raras Tyasurita, Ender Özcan, and Robert John. 2017. Learning heuristic selection using a time delay neural network for open vehicle routing. In *2017 IEEE Congress on Evolutionary Computation (CEC)*. Ieee, 1474–1481.

[41] Ashish Vaswani, Noam Shazeer, Niki Parmar, Jakob Uszkoreit, Llion Jones, Aidan N Gomez, Łukasz Kaiser, and Illia Polosukhin. 2017. Attention is all you need. *Advances in neural information processing systems* 30 (2017).

[42] Thibaut Vidal, Teodor Gabriel Crainic, Michel Gendreau, and Christian Prins. 2013. A hybrid genetic algorithm with adaptive diversity management for a large class of vehicle routing problems with time-windows. *Computers & operations research* 40, 1 (2013), 475–489.

[43] Thibaut Vidal, Gilbert Laporte, and Piotr Matl. 2020. A concise guide to existing and emerging vehicle routing problem variants. *European Journal of Operational Research* 286, 2 (2020), 401–416.

[44] Oriol Vinyals, Meire Fortunato, and Navdeep Jaitly. 2015. Pointer networks. *Advances in neural information processing systems* 28 (2015).

[45] Chenguang Wang and Tianshu Yu. 2023. Efficient Training of Multi-task Neural Solver with Multi-armed Bandits. *arXiv:2305.06361* [cs.LG]

[46] Yongqin Xian, Christoph H Lampert, Bernt Schiele, and Zeynep Akata. 2018. Zero-shot learning—a comprehensive evaluation of the good, the bad and the ugly. *IEEE transactions on pattern analysis and machine intelligence* 41, 9 (2018), 2251–2265.

[47] Xiao-Tong Yuan, Xiaobai Liu, and Shuicheng Yan. 2012. Visual classification with multitask joint sparse representation. *IEEE Transactions on Image Processing* 21, 10 (2012), 4349–4360.

- [48] Yu Zhang and Qiang Yang. 2021. A survey on multi-task learning. *IEEE Transactions on Knowledge and Data Engineering* 34, 12 (2021), 5586–5609.
- [49] Zizhen Zhang, Zhiyuan Wu, Hang Zhang, and Jiahai Wang. 2022. Meta-Learning-Based Deep Reinforcement Learning for Multiobjective Optimization Problems. *IEEE Transactions on Neural Networks and Learning Systems* (2022), 1–14. <https://doi.org/10.1109/TNNLS.2022.3148435>
- [50] Jiuxia Zhao, Minjia Mao, Xi Zhao, and Jianhua Zou. 2020. A hybrid of deep reinforcement learning and local search for the vehicle routing problems. *IEEE Transactions on Intelligent Transportation Systems* 22, 11 (2020), 7208–7218.
- [51] Jianan Zhou, Yaxin Wu, Wen Song, Zhiguang Cao, and Jie Zhang. 2023. Towards Omni-generalizable Neural Methods for Vehicle Routing Problems. In *the 40th International Conference on Machine Learning (ICML 2023)*.
- [52] Tianyu Zhu, Xinhui Shi, Xiangping Xu, and Jinde Cao. 2023. An accelerated end-to-end method for solving routing problems. *Neural Networks* (2023).

A MODEL DETAILS

A.1 Attention

We use the attention mechanism in Vaswani et al. [41], which is a mapping (message passing [26]) of query Q , key K , and value V vectors to an output. For each node i , the query Q_i , key K_i , and value V_i are projections of the input embedding h_i :

$$Q_i = W^Q h_i, K_i = W^K h_i, V_i = W^V h_i. \quad (4)$$

where the parameters W^Q and W^K are of size $(d_k \times d_h)$ and W^V is of size $(d_v \times d_h)$. We compute the compatibility u_{ij} from the queries and keys as follows:

$$u_{ij} = \frac{Q_i^T K_j}{\sqrt{d_k}}. \quad (5)$$

Then we scale the compatibilities u_{ij} using softmax to get attention weights $a_{ij} \in [0, 1]$:

$$a_{ij} = \frac{e^{u_{ij}}}{\sum_j e^{u_{ij}}}. \quad (6)$$

The output vector h_i^o for node i is the combination of the weights a_{ij} and values V_j :

$$h_i^o = \sum_j a_{ij} V_j. \quad (7)$$

A.2 Multi-Head Attention (MHA)

Multi-head attention enables the model to learn diverse information and usually benefits the results. MHA consists of h heads and each head is an attention. It concatenates the results from all heads with a linear projection.

$$\begin{aligned} MHA(h_1, \dots, h_n) &= \text{Concat}(\text{head}_1, \dots, \text{head}_h) W^O \\ \text{head}_i &= \text{Attention}(h_1, \dots, h_n) \end{aligned} \quad (8)$$

where W^O has size $(hd_v \times d_k)$. In our experiments, we use 8 heads with different parameters, and the embedding size is 128. For the attention model in each head, the parameter dimensions are $d_k = d_v = d_h/h = 16$.

A.3 Decoder Details

We use an MHA followed by a SHA in the decoder following Kool et al. [26]. The computing of queries, keys, and values for the MHA are as follows:

$$\begin{aligned} Q_c &= W^Q h_c, K_i = W^K h_i, V_i = W^V h_i, \\ h_c &= \text{Concat}(h_t, a_t), \end{aligned} \quad (9)$$

where h_t is the embedding of the current visited node and a_t is the attribute vector. h_i is the output embedding from the encoder for node i .

In the SHA, we compute the compatibility using equation (5) and clip the results within $[-10, 10]$ with \tanh . We also exclude the masked nodes by setting their compatibility values to $-\inf$:

$$u_{cj} = \begin{cases} 10 \cdot \tanh\left(\frac{q_c^T k_j}{\sqrt{d_k}}\right) & \text{if } j \notin m_t \\ -\inf & \text{otherwise} \end{cases} \quad (10)$$

The output probability of selecting next node is computed as the softmax of the output compatibilities $p_i = \frac{e^{u_i}}{\sum_j e^{u_j}}$.

A.4 Attribute Procedures

Capacity We track the remaining vehicle capacity c_t at each step t , which is initially set to be the capacity of the vehicle $c_1 = 1$ (all demands have been scaled by the capacity). After selecting a new node v_t , we update the remaining capacity as:

$$c_t = c_{t-1} - d_t \quad (11)$$

where c_{t-1} represents the remaining capacity from the previous step, and d_t represents the demand of the selected node in the current step t .

We mask these nodes that have already been visited or have demands that exceed the remaining vehicle capacity.

Time windows We keep track of the current time t_t at each step t , initialized as $t_1 = 0$. After the selection of a new node, we update the current time as:

$$t_t = \max(t_{t-1} + c_{(t-1),t}, e_t) + s_t \quad (12)$$

where t_{t-1} represents the time from the previous step. $c_{(t-1),t}$ represents the distance between the last node and the current node (i.e., the traveling time cost between two nodes). e_t and s_t represent the early time window and the service time at node v_t , respectively.

We mask the visited nodes and the nodes whose time windows cannot be satisfied: 1) when we are unable to visit the node within the feasible time windows starting from the current node, or 2) when visiting the node would result in being too late to return back to the depot.

Duration limit We keep track of the route length l_t at each step t , which is initialized to be zero $l_t = 0$. We update the current route length by adding the route length from the previous step $t-1$ and the distance between the last node and the current node:

$$l_t = l_{t-1} + c_{(t-1),t} \quad (13)$$

We mask the nodes that exceed the duration limit when selected.

Open route We only need a fixed binary indicator for the open route attribute, with $o_t = 1$ representing that the route is open and $o_t = 0$ otherwise. It does not contribute to the masking vector.

However, unlike other attributes, the open route attribute results in a different total distance calculation. The distance between the last node and the depot is not included.

B RESULTS ON ELEVEN VRPS

We present detailed results on eleven VRPs to demonstrate the advantages of our unified model with multi-task learning and attribute composition. We compared the following settings:

- Our unified model with multi-task learning.
- Our unified model with single-task learning on each training VRP.
- Our unified model with single-task learning on the VRP with all training attributes.
- POMO with single-task learning on each training VRP

We also examined the influence of the normalization method and included the results with fine-tuning. Table 6 lists all the results for VRPs of size 50. The top three results for each VRP are highlighted in **bold**. The abbreviations **ST** and **MT** represent single-task learning and our multi-task learning, respectively. **NN**, **BN**, **IN**, and **RN** denote no normalization, batch normalization, instance normalization, and re-zero normalization, respectively. **FT** represents fast fine-tuning. All models were trained on a single RTX 2080Ti GPU. The testing time cost is the duration it takes to solve 5,000 instances for each VRP.

MT vs. ST It is clear from this table that the single-task learning baselines perform similarly to the POMO counterparts. These results come without surprise since the POMO model serves as our base model. The performance of our multi-task learning model is slightly poorer than POMO and single-task learning (which is directly trained on each specific task), but our model has a much better (zero-shot) generalization performance on other seen/unseen tasks. Therefore, our method has a much better average performance across multiple VRP variants. In addition, we only need to build and train one single model to tackle all tasks with various attribute combinations, while single-task learning needs to build a different model for each task. The training budget has been significantly reduced.

Attribute Composition As discussed in the main paper, we directly train the unified model on OVRPBLTW with all attributes taken into account (ST_OVRPBLTW) to demonstrate the benefit of attribute composition. Line 11 in Table 6 lists the results of ST_OVRPBLTW. According to the results, ST_OVRPBLTW can achieve promising performance on the problem it trained on (OVRPBLTW) as well as two VRP variants with similar attributes (OVRPBTW and OVRPLTW). However, its performance becomes extremely poor for the rest VRPs (from simple CVRP to VRPBTW). This observation suggests that ST_OVRPBLTW is over-fitted to CVRPBLTW with all attributes and cannot generalize well to other variants with a subset of attributes. This comparison also confirms the effectiveness and usefulness of our proposed method for learning different VRP variants with attribute composition.

Normalization Line 13 to 16 list the outcomes of the multi-task learning experiment without normalization, batch normalization, instance normalization, and re-zero normalization (BQ-NCO). Overall, we observed that normalization techniques had minimal impact on the results. Surprisingly, even without normalization, the results were already satisfactory. However, it is important to mention that these tests were conducted solely on our unified model with VRPs of size 50. In future work, a comprehensive study is required.

Fine-tuning We conducted fast fine-tuning of ST_CVRP and MT on eleven VRPs. The fine-tuning on each problem costs less

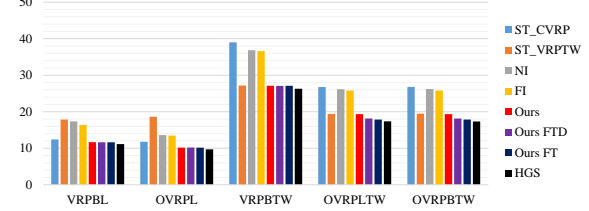


Figure 7: Comparison of the average results (total distances) of different methods on five new VRPs.

than two hours on size 50 and about 5 hours on size 100. The results indicate that the unified model with fine-tuning can yield further performance improvement. With fine-tuning, our unified model achieves the best results with a small gap across all VRPs. See Appendix C for the experimental settings of fine-tuning and more results.

C FAST FINE-TUNING ON UNSEEN VRPS

We conduct experiments to show the performance of our model under fast fine-tuning. The same five unseen VRPs are used: VRP with backhauls and time windows (VRPBTW), VRP with backhauls and duration limitation (VRPBL), open VRP with duration limitations (OVRPL), open VRP with duration limitations and time windows (OVRPLTW), and open VRP with backhauls and time windows (OVRPBTW).

Two different fine-tuning settings are tested: 1) only updating the decoder while keeping the encoder fixed, and 2) updating the entire model. Each epoch is trained using 10,000 instances with a batch size of 64, and 200 epochs are used. The learning rate and weight decay are set to 1e-5 and 1e-6, respectively. The experiments are carried out on the instances of size 100. The entire fine-tuning process with 200 epochs takes approximately five hours, while we note that the model typically converges within the first 50 epochs.

Figure 7 provides a comparison of different methods on the five VRPs in terms of distance. The detailed results are listed in Table 7, where the distance (Dis.), gap to the baseline HGS, and running time of methods are compared on 5,000 instances. The best results are shown in bold.

The abbreviations POMO_CVRP and POMO_VRPTW denote the single-task model (POMO) trained on CVRP and VRPTW instances, respectively. NI and FI represent the nearest and farthest insertion heuristics, and HGS is the SOTA algorithm for VRPs. FTD and FT indicate fine-tuning on the decoder and the entire network, respectively.

Table 6: A summary of results on eleven VRPs with size 50. The top three results on each VRP are in bold. ST and MT represent single-task learning and the proposed multi-task learning, respectively. NN, BN, IN, and RN represent no normalization, batch normalization, instance normalization, and re-zero normalization, respectively. FT represents fast fine-tuning. All the models are trained on a single RTX 2080Ti GPU. The testing time cost is the time cost of solving 5,000 instances on each VRP.

Method	Time Cost										Gap			
	Training	Testing	CVRP	VRPTW	OVRP	VRPB	VRPL	VRPBL	OVRPL	VRPBTLW	OVRPBTW	OVRPBLTW	OVRPBLTW	Average
HGS	/	7 h	0	0	0	0	0	0	0	0	0	0	0	0
LKH3	/	7 h	0.05%	1.29%	0.94%	0.40%	0.96%	/	/	/	/	/	/	0.73%
1 POMO_CVRP	3.8 d	0.11%	38.93%	19.57%	5.38%	0.83%	6.65%	19.65%	39.54%	42.66%	42.48%	43.22%	23.55%	
2 POMO_VRPTW	4.6 d	29.34%	2.52%	66.48%	58.91%	28.06%	53.55%	66.66%	1.60%	7.70%	7.91%	8.00%	30.06%	
POMO	3 POMO_OVRP	4.3 d	15 s	9.28%	45.48%	2.11%	15.79%	9.23%	17.12%	2.38%	44.65%	26.80%	27.32%	20.67%
4 POMO_VRPB	3.9 d	1.85%	42.61%	16.64%	2.10%	1.90%	3.05%	16.75%	43.90%	42.60%	41.55%	41.77%	23.16%	
5 POMO_VRPL	3.9 d	0.49%	38.73%	19.70%	5.48%	0.57%	6.07%	19.44%	39.62%	42.34%	42.41%	43.49%	23.48%	
6 ST_CVRP	4.1 d	0.52%	39.11%	19.52%	5.37%	0.59%	7.07%	19.02%	41.10%	42.34%	41.64%	41.88%	23.47%	
7 ST_VRPTW	4.8 d	39.15%	2.16%	66.23%	67.85%	37.40%	55.30%	65.62%	1.28%	7.83%	7.99%	7.91%	32.61%	
8 ST_OVRP	4.4 d	8.39%	47.46%	2.01%	16.24%	8.49%	17.03%	2.12%	45.92%	25.83%	25.93%	26.76%	20.56%	
9 ST_VRPB	4.1 d	20 s	1.22%	41.50%	16.94%	1.80%	1.59%	3.46%	17.32%	44.67%	43.50%	42.06%	41.40%	23.23%
10 ST_VRPL	4.3 d	0.52%	38.42%	19.56%	8.44%	0.44%	9.67%	19.55%	36.87%	42.08%	43.68%	43.65%	23.88%	
11 ST_OVRPBLTW	5.4 d	22.95%	7.40%	50.29%	43.11%	20.77%	33.84%	48.63%	6.62%	0.90%	0.84%	0.86%	21.47%	
Unified Model	12 ST_CVRP (FT)	4.1 d + 0.6 d	/	23.06%	4.70%	2.83%	0.86%	3.88%	5.03%	21.38%	17.51%	16.74%	14.31%	10.07%
13 MT (NN)	3.9 d	0.58%	2.63%	3.11%	2.34%	0.92%	3.49%	3.27%	1.91%	8.11%	8.28%	8.40%	3.91%	
14 MT (BN)	4.8 d	0.55%	2.66%	3.29%	2.47%	1.11%	3.43%	3.27%	1.82%	7.82%	7.88%	7.82%	3.83%	
15 MT (IN)	4.8 d	20 s	0.42%	2.42%	3.50%	2.05%	1.07%	3.28%	3.18%	1.64%	7.71%	8.95%	8.05%	3.75%
16 MT (RN)	4.3 d	0.55%	2.50%	3.34%	2.24%	0.93%	3.31%	3.35%	2.19%	7.82%	8.08%	8.13%	3.86%	
17 MT (IN, FT)	4.8 d + 0.6 d	0.37%	2.42%	3.04%	2.05%	0.86%	3.15%	3.06%	1.63%	1.90%	1.84%	1.96%	2.02%	

The results indicate that fine-tuning can further improve the performance of our model on new VRPs. Our pre-trained model with fast fine-tuning outperforms all other methods (except for the baseline). The average gap to the baseline HGS is only about 3.4% over the five VRPs. The advantages of fast fine-tuning become more apparent on OVRPLTW and OVRPBTW, which have more attributes and are therefore more complicated. In contrast, fine-tuning only provides minor improvements on VRPBL, OVRPL, and VRPBTW, where zero-shot generalization has already produced satisfactory results.

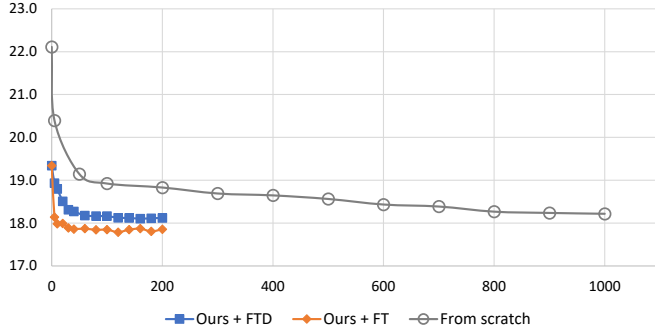


Figure 8: Testing distance vs. epoch number. FTD and FT indicate fine-tuning on the decoder and the entire network of our pre-train unified model, respectively. The curve with grey circles represents training a model from scratch. Each epoch includes 10,000 randomly generated OVRPLTW instances. The testing distance is the average result over 2,000 OVRPLTW instances.

Figure 8 illustrates the convergence of testing distance vs. the number of fine-tuning epochs on OVRPLTW. We compare the performance of fine-tuning the pre-trained model with training a new model from scratch. The experimental settings of training from scratch are the same as that used for fine-tuning. The results demonstrate that fine-tuning based on our pre-trained unified model converges rapidly. The fine-tuning of the entire pre-trained model takes less than 50 epochs (about 1.5 hours) to converge, outperforming the results of training from scratch using 1,000 epochs. The advantage of fast adaptation highlights the significance of our pre-trained unified model.

The results demonstrate the promising generalization ability of our unified model on new problems. In addition to achieving overall acceptable results through direct zero-shot generalization, our proposed unified model can be fine-tuned on new problems with low computational cost, further improving the solution quality.

D EXPERIMENTS ON OUT-OF-DISTRIBUTION INSTANCES

Existing works on neural combinatorial optimization typically assume that the training and testing instances come from the same distribution. Achieving generalization to out-of-distribution cases is often challenging for traditional single-task models. In this section, we investigate the generalization performance of our proposed

multi-task model on three out-of-distribution scenarios of the training problems. All of our experiments are carried out on the problems of size 100.

D.1 CVRP

Basic Settings: The training instance generation for CVRP follows the distribution used in Kool et al. [26]. The coordinates of customers x_i, y_i are randomly sampled in the unit region $[0, 1]$. The demands of customers d_i are randomly selected from $\{1, \dots, 9\}$ and then normalized with respect to the vehicle capacity C . The capacity is set to be $C = 40$ and $C = 50$ for the problem with a size of $n = 50$ and $n = 100$, respectively.

Out-of-Distribution Settings: We evaluate the performance of our model with POMO on CVRP instances with different vehicle capacities. Specifically, we consider seven vehicle capacities: $C = \{20, 30, 40, 50, 60, 70, 80\}$.

Table 8 and Figure 9 show the results on out-of-distribution CVRP instances averaged over 5,000 instances. The better results are in bold, and the gap is calculated using POMO as the baseline. A small gap is preferred and a negative gap indicates that our model outperforms POMO. Except for the results on 50 and 70 (close to that used for generating training instances), our model beats POMO on all the out-of-distribution cases. The advantage of using our unified model is more obvious with the increasing vehicle capacity.

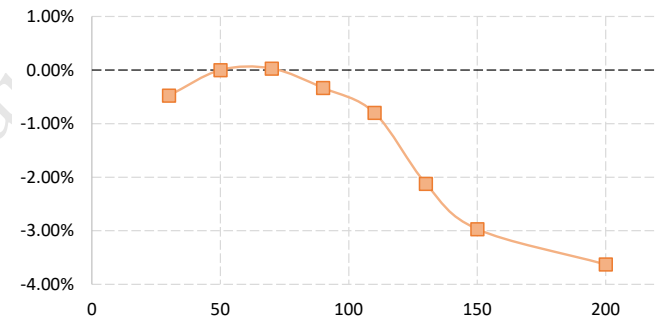


Figure 9: Performance gap between Ours and POMO with respect to different vehicle capacities on CVRP.

D.2 VRPTW

Basic Settings: For VRPTW, we adopt the same settings as those used in Zhao et al. [50]. Specifically, we generate the coordinates, demands, and vehicle capacities using the same procedure as for CVRP. The time windows attributes involve three additional features: 1) the service time s_i , 2) the early time e_i , and 3) the late time l_i . The service time s_i and the length of the time window Δ_i are randomly sampled from a closed interval $[0.15, 0.2]$. The vehicle speed is fixed at $v = 1$ and the maximum time interval of the depot is set to $T = 4.6$. It means that all vehicles must return to the depot before the maximum time interval.

Table 7: Experimental Results on Five New VRPs.

Problem	Method	Dis.	Gap	Time	Problem	Method	Dis.	Gap	Time
VRPBL	HGS	11.15	-	14 h	OVRPLTW	HGS	17.35	-	14 h
	NI	17.38	55.92%	8m		NI	26.16	50.78%	8m
	FI	16.37	46.88%	8m		FI	25.81	48.79%	8m
	POMO_CVRP	12.41	11.37%	1.1m		POMO_CVRP	26.75	54.18%	1.1m
	POMO_VRPTW	17.86	60.27%	1.1m		POMO_VRPTW	19.41	11.88%	1.1m
	Ours	11.65	4.50%	1.2m		Ours	19.34	11.50%	1.2m
	Ours FTD	11.62	4.27%	1.2m		Ours FTD	18.12	4.46%	1.2m
OVRPL	Ours FT	11.64	4.47%	1.2m		Ours FT	17.86	2.94%	1.2m
	HGS	9.71	-	14 h	OVRPBTW	HGS	17.31	-	14 h
	NI	13.61	40.17%	8m		NI	26.24	51.60%	8m
	FI	13.46	38.62%	8m		FI	25.79	48.99%	8m
	POMO_CVRP	11.78	21.35%	1.1m		POMO_CVRP	26.78	54.69%	1.1m
	POMO_VRPTW	18.62	91.78%	1.1m		POMO_VRPTW	19.48	12.51%	1.1m
	Ours	10.15	4.57%	1.2m		Ours	19.32	11.61%	1.2m
VRPBTW	Ours FTD	10.18	4.87%	1.2m		Ours FTD	18.12	4.70%	1.2m
	Ours FT	10.15	4.57%	1.2m		Ours FT	17.84	3.07%	1.2m
	HGS	26.31	-	14 h	Average	HGS	16.36	-	14 h
	NI	36.84	40.05%	8m		NI	24.05	46.95%	8m
	FI	36.59	39.10%	8m		FI	23.60	44.25%	8m
	POMO_CVRP	38.99	48.20%	1.1m		POMO_CVRP	23.34	42.64%	1.1m
	POMO_VRPTW	27.18	3.33%	1.1m		POMO_VRPTW	20.51	25.34%	1.1m
VRPBTW	Ours	27.11	3.05%	1.2m		Ours	17.51	7.03%	1.2m
	Ours FTD	27.08	2.94%	1.2m		Ours FTD	17.03	4.05%	1.2m
	Ours FT	27.11	3.05%	1.2m		Ours FT	16.92	3.40%	1.2m

Table 8: A comparison of our model with single-task POMO on out-of-distribution CVRP instances

Vehicle capacity	30	50	70	90	110	130	150	200
POMO_CVRP	22.913	15.750	12.910	11.480	10.595	10.114	9.824	9.307
Ours	22.804	15.750	12.914	11.441	10.511	9.900	9.532	8.969
Gap	-0.48%	0.00%	0.03%	-0.33%	-0.80%	-2.12%	-2.97%	-3.63%

The early and late times for each customer can be calculated as follows:

$$e_i = \frac{h_i \times c_{0i}}{v}, h_i \in \left[1, \frac{T - s_i - \Delta_i}{c_{0i}} \times v - 1\right] \quad (14)$$

$$l_i = e_i + \Delta_i$$

where c_{0i} denotes the distance between the depot and the i -th customer. This formulation ensures that there is at least one feasible solution for each instance.

Out-of-Distribution Settings: For out-of-distribution testing, we only modify the closed time interval used for sampling service time and time window length. The intervals are as follows: $\{[0.05, 0.1], [0.15, 0.2], \dots, [0.85, 0.9], [0.95, 1.0]\}$.

The results in Table 9 and Figure 10 again reveal that our model is more robust in out-of-distribution cases. We have negative gaps in most cases except for these near training distribution $[0.15, 0.2]$.

D.3 VRPL

Basic Settings: Same as CVRP.

Table 9: A comparison of our model with single-task POMO on out-of-distribution VRPTW instances.

Time Interval	[0.05,0.1]	[0.15,0.2]	[0.25,0.3]	[0.35,0.4]	[0.45,0.5]
POMO_VRPTW	26.230	26.906	28.805	32.327	36.544
Ours	26.390	27.152	29.046	32.174	36.162
Gap	0.61%	0.91%	0.84%	-0.47%	-1.05%
Time Interval	[0.55,0.6]	[0.65,0.7]	[0.75,0.8]	[0.85,0.9]	[0.95,1.0]
POMO_VRPTW	40.650	45.327	49.219	53.300	57.102
Ours	40.136	45.007	48.901	52.815	56.209
Gap	-1.27%	-0.71%	-0.65%	-0.91%	-1.56%

Out-of-distribution Settings: In the training, the duration limit is fixed to $l = 3.0$. We modify the duration limit of each route. The settings used are $l = \{2.9, 3.0, 3.1, 3.2, 3.3, 3.4, 3.5\}$. To better show the effect of the duration limit on the results, we increase the vehicle capacity from 50 to 150 for VRPL. In this way, the number of nodes in each route will increase and the influence of duration limit will be more significant.

Table 10 and Figure 11 show the results. Our model outperforms POMO in all distributions (the reason might be that we have also modified the vehicle capacity). The advantage of our model is more obvious on large duration limits.

Our experiments reveal that our multi-task model displays a strong generalization performance across various distributions. In

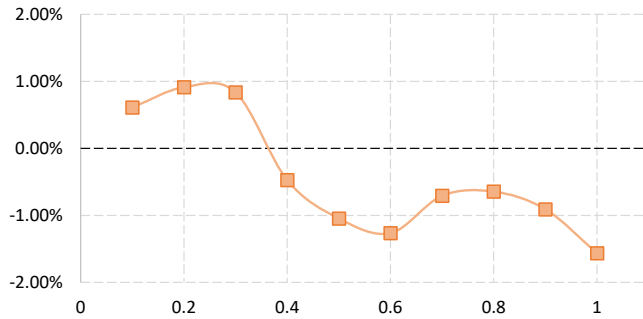


Figure 10: Performance gap between Ours and POMO with respect to different time intervals on VRPTW.

Table 10: A comparison of our model with single-task POMO on out-of-distribution VRPL instances.

Duration	2.9	3	3.1	3.2	3.3	3.4	3.5
POMO_VRPL	10.245	10.145	10.077	10.044	10.019	10.000	9.998
Ours	9.858	9.748	9.683	9.642	9.625	9.601	9.561
Gap	-3.78%	-3.91%	-3.91%	-4.00%	-3.94%	-3.99%	-4.37%

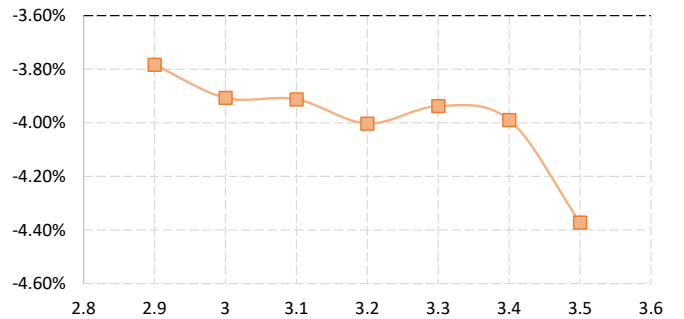


Figure 11: Performance gap between Ours and POMO with respect to different duration limitations on VRPL.

contrast, single-task models perform best only on the test scenarios that share the same distributions as the training data. They are outperformed by the multi-task model when it comes to out-of-distribution scenarios.

We observed that a multi-task model’s advantage becomes more pronounced in extreme cases. For example, on CVRP with a vehicle capacity of 200, our model exhibits a substantial performance gap compared to POMO models. One possible explanation for this is that training a multi-task model with different VRP variants brings diversity. Although it does not specifically represent the utilization of various vehicle capacities, the multi-task model can extract more comprehensive patterns than single-task learning.